Surface Albedo Darkening from Wildfires in Northern Sub-Saharan Africa

C. K. Gatebe[a,b], C.M. Ichoku,[a] R. Poudyal,[a,c] M.O. Román,[a] and E. Wilcox, [d]

[a]*NASA Goddard Space Flight Center, Greenbelt, Maryland, 20771, USA.*

[b]*Universities Space Research Association, Columbia, Maryland, 21228, USA.*

[c]*Science Systems and Applications, Inc., Lanham, Maryland, USA.*

[d]*Desert Research Institute, Reno, Nevada, 89512, USA.*

Correspondence: Charles Gatebe: charles.k.gatebe@nasa.gov

Abstract: Wildfires are recognized as a key physical disturbance of terrestrial ecosystems and a major source of atmospheric trace gases and aerosols. They are known to produce changes in landscape patterns and lead to changes in surface albedo that can persist for long periods. Here, we estimate the darkening of surface albedo due to wildfires in different land cover ecosystems in the Northern Sub-Saharan Africa using data from the Moderate Resolution Imaging Spectroradiometer (MODIS). We determined a decrease in albedo after fires over most land cover types (e.g. woody savannas: (-0.00352 ± 0.00003) and savannas: (-0.00391±0.00003), which together accounted for >86% of the total MODIS fire count between 2003 and 2011). Grasslands had a higher value (-0.00454± 0.00003) than the savannas, but accounted for only about 5% of the total fire count. A few other land cover types (e.g. Deciduous broad leaf: (0.00062 ± 0.00015), and barren: 0.00027 ± 0.00019), showed an increase in albedo after fires, but accounted for less than 1% of the total fires. Albedo change due to wildfires is more important during the fire season (October-February). The albedo recovery progresses rapidly during the first year after fires, where savannas show the greatest recovery (>77%) within one year, while deciduous broadleaf, permanent wetlands and barren lands show the least one-year recovery (56%). The persistence of surface albedo darkening in most land cover types is limited to about six to seven years, after which at least 98% of the burnt pixels recover to their pre-fire albedo.

1. Introduction

Wildfires are recognized as a key physical disturbance of terrestrial ecosystems and a significant source of atmospheric trace gases and aerosols (e.g. Roberts et al., 2009; Andreae & Merlet, 2001; Bremer et al., 2004). Since biomass burning depends primarily on fuel availability that is controlled by mean annual precipitation and soil fertility, intense fire activities are normally observed when vegetation is dry. In Africa, most intense biomass burning is observed in the northern hemisphere between December and February, and in southern Africa between July and November (Scholes & Archer, 1997). These fires are believed to have shaped the savannas vegetation more than any other disturbance (Sheuyange et al., 2005). So there is a strong linkage between biomass burning, weather and climate (cf. Dale et al., 2001; Crutzen and Andreae, 1990).

The extent of wildfires in Africa can be seen clearly from a map of active fire detected by satellite sensors such as the Moderate Resolution Imaging Spectroradiometer (MODIS) at their times of overpass under relatively cloud-free conditions. In the northern Sub-Saharan Africa (NSSA) region, most fires are detected south of the Sahara desert almost across the whole region from west to east (Fig. 1a). Some areas such as Southern Sudan appear to be more fire-prone than others, as nearly every square km of land seems to have been affected by fire at least once between 2003 and 2011 (cf. Figure 1a: inset). During that nine-year period, with approximately two overpasses by Terra every 24 hours (once during the day and once at night), the total MODIS active fire-pixel count at 1-km resolution in the entire NSSA region is about 2.2 million, with an annual average of 242,143 ± 21,664, which is significant. In deed, Africa has the highest frequency of occurrence of fire per land area than any other continent (Ichoku et al., 2008). These fire statistics are likely an underestimate of the actual fire activity, since smaller and cooler fires are probably missed due to the relatively high thresholds used in the MODIS global fire detection algorithm (Giglio et al., 2003; Justice et al., 2002). Some of the factors that can influence fire detection by satellite sensors such as MODIS relate to their orbital and viewing geometry, fire growth rates, fire intensity and size, and fire obscuration by clouds, smoke and atmospheric moisture (Eva & Lambin, 1998). The occurrence of wildfires is more frequent in the savannas (woody savannas and savannas), and account for >86% of the total MODIS fire count between 2003 and 2011 (discussed later in section 3.1; c.f. Table 3, column 2; Fig. 1b). Hence, the spatial-temporal extent of vegetation fires in sub-Saharan Africa is widespread, and creates effects that extend beyond the vegetation it consumes.

There are many possible effects from fires that have been found to manifest through changes in albedo (Govaerts et al., 2002), evapotranspiration (Bosch & Hewlett, 1982; Zhang et al., 2001), rainfall interception (Levia & Frost, 2003), runoff (Farley et al., 2005), and streamflow (Jackson et al., 2005). Therefore, fires can cause multiple effects that operate through changes in albedo, roughness length, and water transport properties from soil to the atmosphere, including leaf area index, stomatal conductance, and rooting depth. Other effects include changes in the carbon mass balance in terrestrial ecosystems, as well as the production of carbonaceous aerosols and trace gases. On a regional scale, surface albedo can play an important role in determining whether aerosols exert a warming or a cooling effect (Ramanathan et al., 2001). However, this albedo dependence is difficult to quantify properly owing to a large spatial and temporal variability as a result of other factors such as seasonal changes in vegetation cover, rainfall, and intensification of land use as measured by population density (Fuller and Ottke, 2002).

This study focuses on changes in surface albedo associated with biomass burning in the NSSA region, where fires are believed to be a major driver of the carbon, energy, and water cycles due to their enormous heat release, and an abundance of gaseous and particulate smoke emissions. The region comprises a wide range of vegetation and climatic zones over a relatively small latitudinal belt from 5–20°N (Fig. 1b), and has become a focal point of debates over desertification, deforestation, and climate change. This study is a part of an interdisciplinary effort investigating the effects of intense biomass burning on the declining regional water resources as exemplified by the drying of Lake Chad. The interdisciplinary study seeks to assess surface, atmospheric and water cycle processes in the region through remote sensing and modelling approaches that integrate research, systems engineering, and applications expertise to best make the connections between various identified processes and phenomena. Such an approach ensures concrete results for societal benefits and climate assessments.

The results of the albedo analysis presented in this paper are expected to provide critical input to various models used in the different aspects of the broader interdisciplinary research. They will be used in the land-surface models to determine the effects of albedo changes due to fires on soil moisture budget, evapotranspiration, infiltration, and runoff, all of which govern the land-surface component of the water cycle. Also, our surface albedo change results will be ingested in atmospheric models, where they will serve as part of the essential input parameters based upon which radiative energy budget estimates are made, both at the surface and at the top of the atmosphere (TOA). As such, these models can better characterize the effects of change in surface albedo due to fires on the atmospheric heating rates of the black carbon (BC) aerosols emitted by fires, which can affect the atmospheric component of the water cycle through the interaction of radiation with surface albedo and the aerosol indirect radiative effects on clouds. Furthermore, information on the spatial and temporal dynamics of the post-fire albedo recovery will be important in modelling the medium- to long-term climate impacts of fires in the NSSA region.

The remainder of this paper is organized into three main sections. Section 2, data and methods, describes the MODIS albedo data, albedo gap filling, and determination of albedo change and recovery. Section 3 presents our results of the albedo change and recovery following fire activities for different land cover types in the NSSA region. Section 4 concludes with a summary of the study.

2. Data and Methods

2.1 MODIS Albedo

Satellites are ideal for providing observations needed for description of surface albedo on a global scale, but we must contend with issues such as uncertainty of the measurements due to atmospheric effects, inadequate sampling (spectral, spatial and temporal), and directionality of these measurements. The global MODIS (Collection 5) albedo product, MCD43A3, (https://lpdaac.usgs.gov/products/modis_products_table/, 1 September 2012) combines measurements from both Terra and Aqua satellites to retrieve directional hemispherical reflectance (black-sky albedo) and bihemispherical reflectance (white-sky albedo) at local solar noon as both spectral (seven narrow spectral bands, http://modis.gsfc.nasa.gov/about/specifications.php, 1 September 2012) and three broadband (0.3–0.7 μm, 0.7–5.0 μm, and 0.3–5.0 μm) quantities.

The albedo is derived from the BRDF (bidirectional reflectance-distribution function) model parameters that are retrieved from all high-quality, cloud-free, atmospherically corrected surface reflectance, acquired over a 16-day period at a spatial resolution of 500 m. The 16-day interval provides an appropriate trade-off between the availability of sufficient angular samples and the temporal stability of the surface (Schaaf et al., 2002; Wanner et al., 1997). However, the assumption of stability becomes more tenuous during periods of strong phenological change such as vegetation green-up, senescence, harvesting, or even snowfall or meltdown, when surface characteristics change abruptly. The synergistic use of MODIS observations from both Terra and Aqua offers an opportunity to increase the angular sampling, and helps to improve the coverage and quality of global BRDF and albedo retrievals (Salomon et al., 2006). Note that Terra has a descending equatorial crossing time of 10:30 a.m., while Aqua has an ascending orbit with a 1:30 p.m. equatorial crossing time. High quality retrievals are obtained during periods of intermittent clear-sky observations by overlapping processing of the data such that retrievals are attempted every eight days (based on all clear sky observations over the 16 days). However, during long periods of clear sky conditions, the 8-day overlapping introduces an autocorrelation between retrievals, since some of the observations wind up being used in more than one period of retrieval (Schaaf et al., 2002).

We used high-quality white-sky broadband albedo (0.3–5.0 µm), whose quality is defined by the BRDF and albedo quality product (MCD43A2), to assess the impact of biomass burning on surface albedo. The white-sky albedo is derived from BRDF measurements, integrated over both incoming and outgoing hemispheres, and does not depend on the illumination and atmospheric conditions. Oftentimes, the high quality retrievals contain significant data gaps, especially in periods of significant cloud cover, where insufficient angular sampling leads to a magnitude inversion rather than a full-model inversion (Schaaf et al., 2002). A full model inversion is attempted only when at least seven cloud-free observations of the surface are available during a 16-day period, and the directional observations adequately sample the view/illumination geometry.

2.2 Gap Filling Method and Validation

As described in Section 2.1, MODIS albedo time series contains data gaps where albedo is not retrieved because of problems such as low data quality, persistent or cloud contamination, and poor illumination conditions, which lead to insufficient angular sampling and a lower accuracy on BRDF and albedo. To address the resulting data gap problem, we developed a simpler algorithm for producing temporally smoothed and spatially complete MODIS white-sky albedo data set. The new gap-filling algorithm first examines each pixel time-series for data gaps and then assigns it one of the five categories determined by the number of consecutive data gaps k in the time-series (k= 1, or 2, or 3, or 4, or ≥4 gaps). For classes with gaps k =1,…, 4, the missing values are determined from Eq. 1:

$$\alpha_t = \alpha_{t-1} + \left(\frac{\alpha_{t+1} - \alpha_{t-1}}{d_{t+1} - d_{t-1}}\right)(d_t - d_{t-1}) \quad (1)$$

where α_t is the missing albedo value on a Julian day, d_t, α_{t-1} is the last existing albedo value in the time series, and α_{t+1} the first albedo value in the time series after the gap. While a majority of the missing values are determined from Eq. 1, the method does not work well when there are more than four consecutive missing values in a time series. In this case, an attempt is made to use neighboring pixels to estimate the missing albedo value within a small window defined by 11 × 11 MODIS 500-m pixels around the missing value, and having the same land cover type as defined by the MODIS Land Cover product (MCD12Q1). If there are no pixels of the same land cover type as the missing value in the selected window, the algorithm progressively increases the search-window size to 31 x 31, or 61 x 61, or 121 × 121, while automatically continuing the search until a suitable albedo match is found. If the algorithm finds no pixels within the maximum search distance (121 × 121 MODIS 500-m pixels), the missing value is replaced by a long-term average albedo derived from the 2003-2011 MODIS albedo of each land-cover type in the entire study region. This approach ensures that every gap is filled with an albedo value.

To verify the efficacy of the new gap filling algorithm to MODIS measurements, we applied it over the Southern Great Plains (SGP) Central Facility site in Oklahoma, USA, over a period of 32 days, centered around 24 June 2007 (Day-of-the-year, DOY, 175), when there was a coincident airborne surface reflectance measurements from NASA's Cloud Absorption Radiometer (CAR; Gatebe et al., 2003; King et al., 1986) taken during the 2007 Cloud and Land Surface Interaction Campaign (CLASIC'07; Román et al. 2011). That period was dominated by cloudy sky and heavy rainfall in the region, resulting in a lot of missing albedo values (Román et al., 2011) that had to be filled to create a good dataset to evaluate the new gap filling method. Thus, we used the coincident retrievals from CAR to make first-order evaluation of the gap filled approach (c.f. Table 1; Fig. 2, MODIS albedo2). We also compared our method to the MODIS temporally smoothed and spatially continuous albedo method by Gao et al., (2008) (c.f. Table 1; Fig. 2, MODIS albedo1). Note that we used the full expression for all retrievals from aircraft (CAR) and MODIS gap filled approaches (albedo1 and albedo2), as described in Román et al, (2010). Although MODIS albedo values are systematically biased low against aircraft/CAR albedo and tower based albedo by about 15–20%, the two gap-filling methods (albedo1 and albedo2) agree to within 4–5% (cf. Table 1), but the new approach is simpler and uses mainly the most recent values on either side of the gap and land cover to fill the missing values. On the other hand, MODIS gap filling approach (Gao et al., 2008) is much more rigorous and normally fit at least 18 months to adequately capture the phenology and bridge a gap. These systematic differences should have little or no impact on the determination of albedo change due to fires.

2.3 Determination of albedo change due to fires

The albedo change caused by biomass burning was determined at the pixel level for each land cover type using the 2003-2011 MODIS albedo data record in the entire NSSA region on a monthly basis. A pixel was considered burned when an active fire was reported in the MODIS Level-3, 8-day daily active fire product (MOD14A2) at the 1 km grid cell and at all the fire detection confidence (low-confidence fire, nominal-confidence fire, or high-confidence fire). The decision to consider fires in all confidence classes was meant to boost the number of burnt pixels, especially during the non-fire season months. The study focuses more on the albedo changes during fire season. Here, we define the average albedo change $\Delta\overline{\overline{\Omega}}_c$ due to vegetation fires for land cover type c as:

$$\Delta\overline{\overline{\Omega}}_c = \overline{\Omega}_c - \overline{\Omega}_{c,0} \qquad (2)$$

where $\overline{\Omega}_{c,0}$ is the albedo of unburned pixels (c.f. Table 2), before or when a fire is reported, averaged over many pixels of the same land cover type c, and $\overline{\Omega}_c$ is an albedo of the burned pixels, 24 days after fire is reported, averaged over many pixels of the same land cover type *c*. Table 3 shows the monthly albedo change derived from various major land cover types in the NSSA region, which constitute 99.7% of the land area, and averaged over nine years of MODIS data from 2003-2011. Note that monthly values are defined by the average of the 8-day retrievals that fall in a calendar month. The standard deviation in each case (Table 3) represents a temporal and spatial variability of the albedo change.

3. Influence of biomass burning on albedo

3.1 Albedo changes caused by biomass burning

We estimated changes in the albedo after vegetation fires for 11 major land ecosystem types in Africa, which are defined by the International Geosphere and Biosphere Programme (IGBP) and applied to the global 1-km MODIS data (cf. Fig. 1b; Friedl et al., 2002) – referred to here as the MODIS land cover. Barren or sparsely vegetated lands occupy a large area of the northern Sub-Saharan Africa, 25%, followed by woody savannas, 15%, grassland, 15%, savannas, 11%, open shrubland, 11%, evergreen broadleaf, 10%, cropland or natural vegetation, 8%, closed shrubland, 2%, cropland, 2%, persistent wetland, 0.6%, deciduous broadleaf and others, ~0.003%. As noted earlier, the occurrence of fires is most frequent in the savannas (woody savannas and savannas), which accounted for over 86% of the total MODIS fire count between 2003-2011 (cf. Table 3, column 2; Fig. 1b). As shown in Figure 3, most fires in the NSSA occur between October and March, with the peak for some cover types around January or November. Barren or desert land cover type has a peak around May, but this may be a false peak given that fire detection over barren or desert is quite a challenge and oftentimes contains more false alarms compared to other land cover types (c.f. Giglio et al., 2003).

The albedo change caused by fires varies by ecosystem type as depicted in Fig 4, and detailed in Table 3. Each value represents an average of many burnt pixels of the same land cover type and over nine years (2003-2011). The standard deviation accounts for temporal and spatial variability of the albedo change due to fires. Some ecosystems show large values of the standard deviation partly because of post-fire changes in surface albedo associated with dissipation of charcoal and ash, and vegetation regrowth over the 24 days period used to calculate monthly post-fire albedo change (cf. Jin & Roy, 2005). Figure 4a shows total albedo change for all months in each land cover type, which show an increase in albedo except in barren and evergreen broadleaf forests. But given that most fires occur between October and February in the NSSA region (cf. Fig. 3), we decided to aggregate albedo change values for the fire season months (October-February).

Figure 4b shows the albedo change during the biomass burning season, where most land cover types now show a decrease in albedo after fires, except for a few land cover types (e.g. deciduous broadleaf forests). Both evergreen broadleaf forests and grasslands show the highest albedo decrease ((-0.00590 ± 0.00015) and (-0.00454 ± 0.00003), respectively), followed by savannas (-0.00352 ± 0.00003), croplands/natural vegetation (-

0.00374±0.00002), woody savannas (-0.00352 ± 0.00003), open shrublands (-0.00266±0.00002), and croplands (-0.00110 ± 0.00003). The four land cover types that show an increase after fires are permanent wetlands (0.00340±0.00010), closed shrublands (0.00144 ± 0.00003), deciduous broadleaf forest (0.00062±0.00008), and barren (0.00027±0.00019). The change in albedo associated with fires is more important where most fires are reported (e.g. woody savannas (48.69%), savannas (37.73)%, crop/natural vegetation (5.59%) and grasslands (4.78%)), which together accounted for about 97% of all the MODIS fires detected between 2003 and 2011. Some studies have suggested that the observed differences in albedo change among different land covers are likely related to differences in fuel composition and combustion characteristics, with generally higher combustion completeness observed in grasslands than woodlands (Jin & Roy, 2005; Roy et al. 2008; Hoffa et al., 1999).

Fires during the main burning season reduce the albedo of savannas, woody savannas, crop/natural vegetation and grasslands as described above and shown in figure 4b. The relatively few fires during the northern hemisphere summer months cause an increase in albedo that is sufficiently large to dominate the annual average of the albedo perturbation for all fire events shown in figure 4a. However, we note that the uncertainties in both the albedo and the albedo perturbation reported in tables 2 and 3 during the summer months for these land surface types are larger than the uncertainties for the winter months. Thus, we conclude that the albedo reduction during the main fire season for these land surface types is the more robust result. Higher spatio-temporal variability in the albedo during the summer months accounts for greater uncertainty in characterizing the undisturbed albedo during these months. Quantifying the albedo perturbation during these months is further hampered by the relatively few fire events.

Figure 5 illustrates further the importance of albedo change in the fire months (October – February). While albedo change in July is high (Fig. 5a), probably caused by uncertainties of rapidly changing albedo that is correlated with the peak growing season, the contribution is negligible when the monthly albedo changes are weighted by the fractional fire count in each month (Fig. 5b). The albedo perturbations during the fire months (Oct-Feb) stand out more prominently. Therefore, the albedo increase shown in Fig 4a is due to uncertainties associated with other disturbances, while fires reduce or darken the surface albedo as observed during the fire season (Fig. 4b). Additionally, the albedo decrease after fires in February and December is associated with peak burning period of certain land cover types depicted in Fig 3a (e.g. savannas, woody savannas, and croplands), probably related to post-fire albedo darkening due to dissipation of charcoal and ash, or vegetation growth. While the albedo increase after fires in January, October, and November is associated with peak burning period of other land cover types depicted in Fig 3b (e.g. grasslands, shrublands and barren), probably related to the reduced vegetation moisture content in the fall and winter, and resultant increasing combustion completeness during burning that leads to more exposure of the underlying soils with higher albedo. This is consistent with the findings of Hoffa et al. (1999) deduced from experimental burning, where decreasing vegetation moisture content and increasing fire line intensity were noted as the dry season progressed. Full details of albedo change by month and land cover types are given in Table 3. The magnitude of albedo perturbations seen here (relative differences: -7% to 6 %) is consistent with results from other studies (e.g. Govaerts et al. 2002) over the fire affected areas in the NSSA region (5°N–10°N), where relative differences were found to range between -8% and -5%.

3.2 Post-fire albedo recovery

In this section, we will describe results of the post-fire persistence of surface albedo changes in different ecosystems. This is deduced from the time it takes albedo to go back to its pre-fire value. Our approach involves tracking albedo at the pixel level comparing both burned and unburned (control) cases for the same ecosystem. The unburned case was carefully selected from neighbouring pixels and same land cover type that show similar albedo characteristics over an extended period of time (at least two years), under similar conditions. Figure 6a shows a plot of albedo time series of both burned and unburned savannas pixels, before and after fires for a period of about 3 years. Note that the interval between data points is eight days. Figure 6b shows the same data, but zooming into the fire period in order to show details of the albedo recovery after the fires. The pre-fire albedo values exhibit a seasonal trend consistent with the vegetation phenology changes from senescence to greenup, before and after the northern hemisphere winter in October–February. The corresponding post-fire albedo values follow a similar trend, but have consistently lower values after the fire is detected (gray-shaded region in Fig. 6a&b). Since the points represent albedo every eight days, the recovery period in this case takes 288 days or about a year. We used this approach to determine how long it took a burnt pixel to return to the pre-fire albedo levels compared to a control pixel, which mimicked how the burnt pixel would have behaved over several years without fires.

Figure 7 and Table 4 show post-fire albedo recovery of different land cover types in northern sub-Saharan Africa for burn events that took place in 2003 tracked cumulatively at 3-month intervals over a period of seven years. At each step, we normalized by the total number of tracked pixels in each land cover type. During the first year after the fires, some biomes such as croplands, closed broadleaf forests, deciduous broad leaf forests and barren or sparse vegetation experience a more rapid albedo recovery. Others such as grassland, savannas, and woody savannas take a slower recovery path. Over 60% of the burnt pixels recover their albedo to pre-fire period for all the biomes during the first year after the burn. By the end of the second year after fires, over 80% of the burnt pixels recover their albedo to pre-fire period, with some biomes such as deciduous broadleaf and closed shrublands showing 100% albedo recovery. For the savannas and woody savannas, where 86% of burning takes place, >97% of the burnt pixels take at least five years to recover their albedo to pre-fire period. Over 97% of the evergreen broadleaf forests burnt pixels took at least six years to recover their albedo to pre-fire period.

4. Conclusions

We estimated the change of surface albedo due to fires over different land cover types in the Northern Sub-Saharan Africa using data from the Moderate Resolution Imaging Spectroradiometer (MODIS) from 2003–2011. We determined a decrease in albedo over most land cover types due to fires (e.g. woody savannas (-0.00352 ± 0.00003) and savannas (-0.0.00391±0.00003), which accounted for >86% of the total MODIS fire count between 2003 and 2011. Grasslands had a higher value (-0.00454± 0.00003) than the savannas, but accounted for only about 5% of the total fire count. A few other land cover types (e.g. Deciduous broad leaf: 0.00062 ± 0.00015 and barren: 0.00027 ± 0.00019) showed an increase in albedo after fires, but accounted for less than 1% of the total fires. The observed monthly albedo change for various biomes in NSSA is variable, while the largest values observed in July, probably caused by uncertainties due to rapidly changing albedo and correlated with the peak growing season. During the fire season the monthly albedo decrease is correlated with peak fire count of some land cover types (e.g. savannas), related to post-fire albedo darkening due to dissipation of charcoal and ash, or vegetation regrowth. The albedo increase is correlated with peak fire count of the other land cover types (e.g. grasslands), related to the reduced vegetation moisture content in the fall and winter, and resultant increasing combustion completeness during burning that leads to more exposure of the underlying soils with higher albedo. The albedo recovery after fires progresses rapidly in year one, with the savannas leading in the recovery (>77%) and deciduous broadleaf, permanent wetlands and barren showing the least recovery (56%). The persistence of surface albedo darkening or brightening is limited to about six to seven years, where at least 98% of the burnt pixels recover to their pre-fire albedo for all land cover types.

Acknowledgements

This research was supported by the Science Mission Directorate of the National Aeronautics and Space Administration as part of the Interdisciplinary Studies (IDS) conducted through the Radiation Sciences Program under Hal B. Maring. We would like to thank C. Schaaf and J. Wang for insightful comments. This work was performed under NASA Grant NNX11AQ98G.

References

Andrea, M. O. & Merlet, P. (2001). Emission of trace gases and aerosols from biomass burning. *Global Biogeochemical Cycles*, 15, 955–966.

Bremer, H., Kar, J., Drummond, J. R., Nichitu, F., Zou, J., Liu, J., Gille, J. C., et al. (2004). Spatial and temporal variation of MOPITT CO in Africa and South America: A comparison with SHADOZ ozone and MODIS aerosol. *Journal of Geophysical Research*, 109 (D12304). doi:10.1029/2003JD004234.

Bosch, J. M., & Hewlett, J. D. (1982). A review of catchment experiments to determine the effect of vegetation changes on water yield and evapotranspiration. *Journal of Hydrology,* 55, 3–23.

Crutzen, P. J., & Andreae, M. O. (1990). Biomass burning in the tropics: Impacts on atmospheric chemistry and biogeochemical cycles. *Science*, 250, 1669–1778.

Dale, V. H., Joyce, L. A., Mcnulty, S., Neilson, R. P., Ayres, M. P., Flannigan, M. D., et al. (2001). Climate Change and Forest Disturbances. *BioScience,* 51(9), 723–734.

Eva, H., & Lambin, E. F. (1998). Remote sensing of biomass burning in tropical regions: sampling issues and multisensor approach. *Remote Sensing of Environment*, 64, 292–315.

Farley, K. A., Jobbágy, E. G., & Jackson, R. B. (2005). Effects of afforestation on water yield: a global synthesis with implications for policy. *Global Change Biology*, 11, 1565–1576.

Friedl, M. A., McIver, D. K., Hodges, J. C. F., Zhang, X. Y., Muchoney, D., Strahler, A. H., et al. (2002). Global land cover mapping from MODIS: Algorithms and early results. *Remote Sensing of Environment*, 83, 287–302.

Fuller, O. D., & Ottke, C. (2002). Land cover, rainfall and land-surface albedo in West Africa. *Climatic Change,* 54, 181–204.

Gao, F., Morisette, J. T., Wolfe, R. E., Ederer, G., Pedelty, J., Masuoka, E., Myneni, R., Tan, B., & Nightingale, J. (2008). An Algorithm to produce temporally and spatially continuous MODIS-LAI time series. *IEEE Geoscience and Remote sensing Letters*, 5 (1), 60–64.

Gatebe, C. K., King, M. D., Platnick, S., Arnold, G. T., Vermote, E. F., & Schmid, B. (2003). Airborne spectral measurements of surface-atmosphere anisotropy for several surfaces and ecosystems over southern Africa. *Journal of Geophysical Research*, 108, 8489. doi:10.1029/2002JD002397.

Giglio, L., Descloitres, J., Justice, C. O., & Kaufman, Y. (2003). An enhanced contextual fire detection algorithm for MODIS. *Remote Sensing of Environment*, 87, 273–282.

Govaerts, Y. M., Pereira, J. M., Pinty, B., & Mota, B. (2002). Impact of fires on surface albedo dynamics over the African continent. *Journal of Geophysical Research*, 107 (D22, 4629), doi:10.1029/2002JD002388.

Hoffa, E. A., Ward, D. E., Hao, W. M., Susott, R. A., & Wakimoto, R. H. (1999). Seasonality of carbon emissions from biomass burning in a Zambian savanna. *Journal of Geophysical Research*, 104(D11), 13841–13853.

Ichoku, C., Giglio, L., Wooster, M. J., & Remer, L. A. (2008). Global characterization of biomass-burning patterns using satellite measurements of radiative energy, *Remote Sensing of Environment*, 112, 2950–2962.

Jackson, R. B., Jobbágy, E. G., Avissar, R., Roy, S. B., Barrett, D. J., Cook, C. W., et al. (2005). Trading water for carbon with biological sequestration. *Science*, 310, 1944–1947.

Jin, Y., & Roy, D. P. (2005). Fire-induced albedo change and its radiative forcing at the surface in northern Australia. *Geophysical Research Letters*, 32, L13401. doi:10.1029/2005GL022822.

Justice, C. O., Giglio, L., Korontzi, S., Owens, J., Morisette, J., Roy, D., Descloitres, J., Alleaume, S., Petitcolin, F., & Kaufman, Y. (2002). The MODIS fire products, *Remote Sensing of Environment*, 83, 244–262.

King, M. D., Strange, M. G., Leone, P., & Blaine, L. R. (1986). Multiwavelength scanning radiometer for airborne measurements of scattered radiation within clouds. J*ournal of Atmospheric and Oceanic Technology*, 3, 513–522.

Levia, D. F., & Frost, E. E. (2003). A review and evaluation of stemflow literature in the hydrologic and biogeochemical cycles of forested and agricultural ecosystems. *Journal of Hydrology*, 274, 1–29.

Ramanathan, V., Crutzen, P. J., Kiehl, J. T., & Rosenfeld, D. (2001). Aerosols, climate, and the hydrological cycle. *Science*, 294, 2119–2124, DOI: 10.1126/science.1064034.

Roberts, G., M. J. Wooster, and E. Lagoudakis (2009). Annual and diurnal African biomass burning temporal dynamics, *Biogeosciences*, 6, 849–866.

Román, M. O., Gatebe, C. K., Schaaf, C., Poudyal, R., Wang, Z., & King, M. D. (2011). Variability in surface BRDF at different spatial scales (30 m–500 m) over a mixed agricultural landscape as retrieved from airborne and satellite spectral measurements. *Remote Sensing of Environment*, 115, 2184-2203. doi:10.1016/j.rse.2011.04.012.

Román, M. O., Schaaf, C. B., Lewis, P., Gao, F., Anderson, G. P., Privette, J. L., Strahler, A. H., Woodcock, C. E., Barnsley, M. (2010). Assessing the coupling between surface albedo derived from MODIS and the fraction of diffuse skylight over spatially-characterized landscapes. Remote Sensing of Environment, 114, 738–760.

Roy, D. P., Boschetti, L., Justice, C. O., & Ju, J. (2008). The Collection 5 MODIS Burned Area Product - Global Evaluation by Comparison with the MODIS Active Fire Product. *Remote Sensing of Environment*, 112, 3690–3707.

Salomon, J., Schaaf, C. B., Strahler, A. H., Gao, F., Jin, Y. (2006). Validation of the MODIS bidirectional reflectance distribution function and albedo retrievals using combined observations from the Aqua and Terra Platforms, IEEE Transactions of. Geoscience and Remote Sensing, 44 (6), 1555–1565.

Schaaf, C. B., Gao, F., Strahler, A. H., Lucht, W., Li, X., Tsang, T., Strugnell, N. C., et al. (2002). First operational BRDF, albedo and aadir reflectance products from MODIS. *Remote Sensing of Environment*, 83, 135–148.

Sheuyange, A., Oba, G., & Weladji, R. B. (2005). Effects of anthropogenic fire history on savanna vegetation in northeastern Namibia. *Journal of Environmental Management*, 75, 189–198.

Scholes, R. J., & Archer, S. R. (1997). Tree–grass interactions in savannas. *Annual Review of Ecological Systems*, 28, 517–544.

Wanner, W., Strahler, A. H., Hu, B., Lewis, P., Muller, J.-P., Li, X., Schaaf, C. L. B. & Barnsley, M. J. (1997). Global retrieval of bidirectional reflectance and albedo over land from EOS MODIS and MISR data: Theory and algorithm. *Journal of Geophysical Res*earch, 102, 17143–17162.

Zhang, L, Dawes, W. R., & Walker, G. R. (2001). Response of mean annual evapotranspiration to vegetation changes at catchment scale. *Water Resources Research*, 37, 701–708.

Table 1: Accuracy and uncertainty values resulting from a 32-day comparison between airborne (CAR) and satellite-derived (MODIS) albedos using two different gap-filling approaches.

a. All Days	10°≤ SZA ≤45° (n=289)			45°≤ SZA ≤75° (n=193)		
DOY 159–190	Aircraft/(CAR)	MODIS/albedo1	MODIS/albedo2	Aircraft/(CAR)	MODIS/albedo1	MODIS/albedo2
Accuracy	0.0042	-0.0286	-0.0333	-0.0096	-0.0495	-0.0570
Uncertainty	0.0082	0.0296	0.0341	0.0184	0.0526	0.0589

Table 2: Albedo of unburnt pixel from MODIS (2003-2011) for different land cover types in the NSSA

Landcover	Jan	Feb	Mar	April	May	June	July	Aug	Sept	Oct	Nov	Dec
Barren/ sparsely veg.	0.169± 0.032	0.187± 0.028	0.196± 0.004	0.168± 0.039	0.176± 0.034	0.187± 0.040	0.208± 0.027	0.187± 0.028	0.174± 0.034	0.212± 0.033	0.201± 0.036	0.191± 0.075
Savannas	0.135± 0.004	0.147± 0.002	0.159± 0.002	0.160± 0.005	0.162± 0.005	0.158± 0.005	0.151± 0.013	0.143± 0.019	0.135± 0.014	0.147± 0.003	0.130± 0.003	0.130± 0.002
Woody Sa-vannas	0.128± 0.004	0.137± 0.002	0.148± 0.003	0.151± 0.005	0.155± 0.005	0.157± 0.007	0.145± 0.014	0.147± 0.019	0.137± 0.009	0.144± 0.002	0.130± 0.002	0.126± 0.003
Evergreen broadleaf	0.123± 0.003	0.127± 0.002	0.140± 0.006	0.140± 0.005	0.138± 0.005	0.148± 0.008	0.140± 0.014	0.138± 0.009	0.140± 0.017	0.130± 0.014	0.130± 0.007	0.120± 0.006
Grassland	0.155± 0.007	0.165± 0.004	0.175± 0.004	0.180± 0.006	0.187± 0.012	0.189± 0.012	0.166± 0.015	0.158± 0.012	0.155± 0.017	0.161± 0.006	0.145± 0.003	0.151± 0.004
Open shru-bland	0.167± 0.006	0.184± 0.006	0.195± 0.015	0.193± 0.011	0.201± 0.004	0.209± 0.016	0.219± 0.032	0.228± 0.054	0.183± 0.022	0.164± 0.009	0.155± 0.008	0.164± 0.007
Crop/nat. vegetation	0.155± 0.003	0.162± 0.003	0.171± 0.003	0.176± 0.007	0.178± 0.007	0.174± 0.006	0.157± 0.014	0.161± 0.017	0.152± 0.011	0.157± 0.003	0.151± 0.004	0.155± 0.003
Closed shrub	0.146± 0.004	0.153± 0.004	0.164± 0.004	0.161± 0.008	0.158± 0.009	0.158± 0.020	0.157± 0.015	0.136± 0.013	0.130± 0.012	0.149± 0.004	0.140± 0.003	0.143± 0.004
Cropland	0.155± 0.004	0.164± 0.006	0.170± 0.004	0.172± 0.004	0.167± 0.006	0.170± 0.015	0.157± 0.014	0.144± 0.017	0.146± 0.018	0.160± 0.008	0.148± 0.006	0.152± 0.004
Persistent wetland	0.117± 0.012	0.126± 0.006	0.137± 0.007	0.140± 0.006	0.141± 0.006	0.144± 0.016	0.142± 0.016	0.132± 0.028	0.114± 0.015	0.134± 0.010	0.122± 0.010	0.116± 0.008
Deciduous broadleaf	0.140± 0.004	0.145± 0.004	0.153± 0.005	0.153± 0.002	0.151± 0.013	0.147± 0.031	0.136± 0.012	0.114± 0.033	0.150± 0.024	0.146± 0.011	0.139± 0.003	0.139± 0.004

Table 3: Fire frequency and albedo change due fires from MODIS (2003-2011) for different land cover types in the NSSA

		Albedo Change (x 10^{-5})											
	Fire count (%)	Jan	Feb	Mar	Apr	May	Jun	Jul	Aug	Sep	Oct	Nov	Dec
Barren/ sparsely veg.	0.18	4.4± 9.0	-0.2± 7.5	0.3± 5.2	0.7± 10.7	-4.8± 13.0	-1.7± 19.4	0.7± 9.6	0.3± 4.4	0.7± 6.8	-1.8± 7.3	0.1± 14.1	-2.2± 5.4
Savannas	37.73	-2.0± 3.5	-3.9± 4.3	0.4± 5.0	1.0± 3.5	2.1± 3.5	3.2± 4.8	4.4± 8.1	-2.4± 9.8	-0.3± 6.0	4.5± 4.8	0.3± 2.6	-2.7± 3.4
Woody Savannas	48.69	-1.6± 3.7	-3.6± 4.0	-1.1± 3.4	-0.2± 2.5	-0.1± 2.5	2.5± 5.1	6.0± 15.0	-0.2± 10.4	1.0± 7.4	3.0± 3.7	0.3± 2.8	-1.6± 3.2
Evergreen broad-leaf	0.71	1.4± 3.4	-4.9± 7.2	0.5± 6.1	-1.0± 5.9	-3.5± 8.7	-4.0± 12.0	2.7± 18.9	2.0± 14.5	5.3± 16.0	-1.3± 15.0	-0.2± 4.9	-0.9± 4.3
Grassland	4.78	-0.5± 2.8	-3.2± 4.1	-0.5± 3.8	1.7± 3.9	-1.6± 3.7	3.1± 6.9	8.2± 14.3	4.5± 12.5	-2.3± 4.9	-1.1± 3.2	1.0± 3.4	-0.7± 3.7
Open shrubland	0.67	0.4± 3.1	-2.3± 3.8	-0.7± 4.5	1.2± 5.2	-1.3± 3.5	4.7± 7.1	7.3± 10.4	2.6± 12.3	-1.7± 6.3	-0.6± 2.6	1.1± 3.2	-1.3± 3.2
Crop/nat. vegeta-tion	5.59	-0.5± 2.4	-3.0± 3.0	0.5± 4.6	0.2± 3.0	-0.2± 4.0	4.2± 7.3	1.0± 14.1	3.4± 15.2	0.8± 6.5	-0.6± 1.6	0.7± 3.3	-0.4± 2.8
Closed shrub	0.16	0.9± 3.0	-3.8± 5.2	2.1± 3.6	3.0± 4.8	0.3± 7.4	0.4± 13.2	7.9± 15.8	0.9± 11.8	3.6± 7.6	4.0± 4.1	1.7± 2.3	-1.3± 4.3
Cropland	0.89	0.9± 3.8	-3.3± 3.7	0.9± 6.0	1.6± 4.5	-2.0± 5.2	1.3± 7.6	0.9± 13.0	3.2± 16.7	0.7± 6.0	-0.1± 3.3	0.5± 5.0	0.9± 2.3
Persistent wetland	0.34	4.1± 4.8	-3.4± 4.8	-0.4± 5.9	2.0± 4.9	-0.3± 10.0	-2.0± 7.1	4.6± 16.2	-1.8± 7.8	1.2± 7.8	0.9± 9.9	0.4± 5.8	1.4± 7.2
Deciduous broad-leaf	0.26	-0.9± 2.6	-3.3± 4.5	-1.0± 5.0	0.4± 5.3	2.7± 9.3	0.2± 5.3	2.4± 6.9	-0.4± 4.6	-0.2± 1.1	6.4± 10.7	0.0± 4.8	-1.6± 3.3

Table 4: Post-fire albedo recovery after every three months

	No of burnt pixels with full-albedo recovery (%)										
Yrs	Savan nas	Woody Savanas	Grasslands	Cropland	Barren	Cropland Nat. Veg	Ever-green-broad-leaf	Open Shrubl ands	Closed Shru-blands	Perma-nent Wetlands	Decidu-ous broad-Leaf
0.25	49.25	41.18	34.47	24.58	22.07	45.94	25.46	35.92	24.93	23.47	20.92
0.49	55.47	44.61	43.71	49.49	31.06	53.61	33.72	43.69	33.99	33.60	30.09
0.74	60.94	53.06	51.35	62.63	43.05	62.12	45.87	54.13	45.61	45.87	42.69
0.99	77.93	81.77	73.02	71.38	55.59	79.79	58.26	64.32	56.66	56.53	55.87
1.23	83.71	88.01	76.87	77.10	61.58	82.39	64.91	69.17	62.61	63.73	62.18
1.48	84.13	88.21	77.45	79.12	64.31	83.17	67.20	71.60	65.16	66.93	65.04
1.73	84.64	88.49	78.91	82.32	68.66	84.15	70.87	75.49	69.69	70.93	69.91
1.97	87.99	91.99	88.73	85.35	73.02	88.17	75.92	79.61	74.22	76.27	74.50
2.22	92.00	94.17	90.25	87.21	76.57	91.10	78.90	82.52	78.75	79.20	77.94
2.47	92.18	94.21	90.47	87.88	77.11	91.16	79.59	83.01	79.32	79.47	78.51
2.71	92.31	94.33	90.91	89.56	79.29	91.62	81.42	84.71	81.30	81.60	80.80
2.96	93.21	95.49	94.11	91.58	85.01	94.28	84.40	87.62	84.99	85.07	84.53
3.21	95.75	96.83	94.98	93.43	87.74	95.19	86.70	89.81	87.82	87.73	87.39
3.45	95.88	96.90	95.56	94.44	89.37	95.52	88.07	91.26	89.52	89.60	89.11
3.70	95.93	96.99	95.78	95.45	91.28	95.78	89.91	92.96	91.50	91.47	91.40
3.95	96.20	97.31	97.16	96.46	93.19	96.56	91.51	94.42	93.48	93.33	93.41
4.19	97.71	98.26	97.96	97.14	94.55	97.21	93.35	95.15	94.90	94.40	94.84
4.44	97.76	98.30	98.11	97.31	95.37	97.40	94.04	95.87	95.47	95.20	95.70
4.68	97.83	98.34	98.11	97.98	96.46	97.60	94.95	96.84	96.60	96.27	96.85
4.93	98.06	98.55	98.55	98.15	97.00	98.05	95.18	97.09	96.88	96.53	97.13
5.18	99.35	99.30	99.20	98.65	98.09	98.64	96.10	98.06	98.02	97.60	97.99
5.42	99.39	99.32	99.27	98.99	98.37	98.64	96.33	98.30	98.30	97.87	98.28
5.67	99.41	99.36	99.27	98.99	98.37	98.64	96.33	98.30	98.30	97.87	98.28
5.92	99.50	99.47	99.71	99.16	98.91	98.77	96.79	99.03	98.87	98.40	98.85
6.16	99.87	99.90	99.93	99.66	99.73	99.48	97.71	99.76	99.72	99.20	99.71
6.41	99.88	99.91	100.00	99.83	100.00	99.55	97.94	100.00	100.00	99.47	100.00
6.66	99.88	99.91	100.00	100.00	100.00	99.94	97.94	100.00	100.00	99.47	100.00

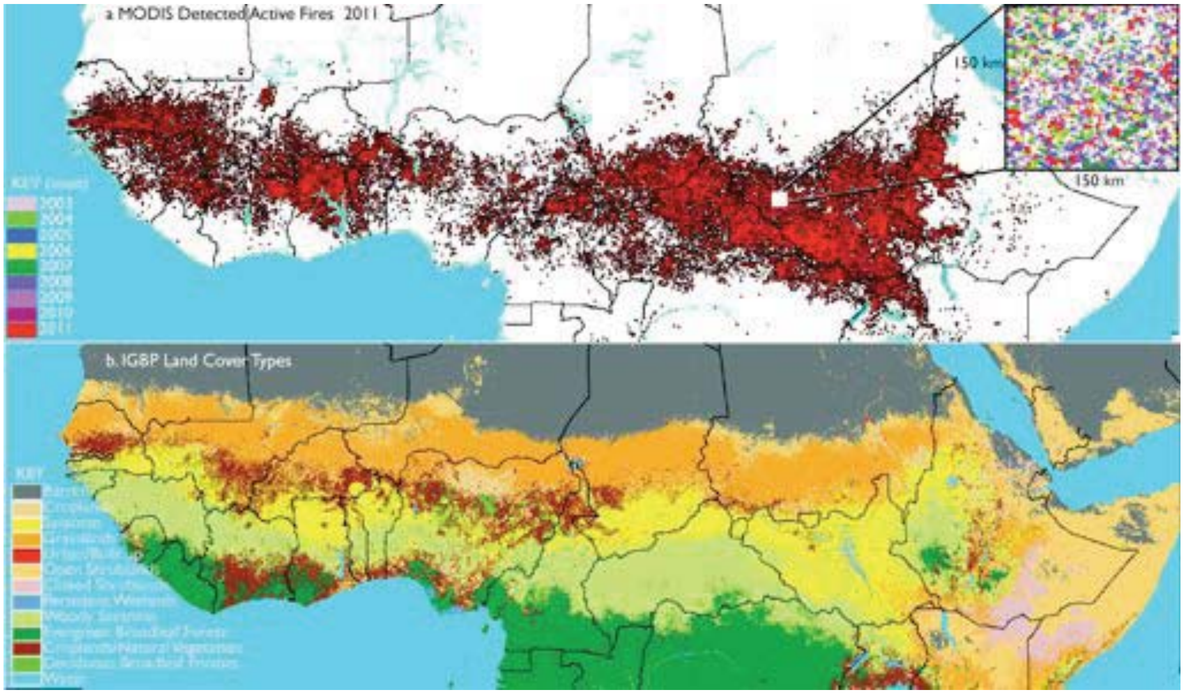

Fig. 1. a. Spatial distribution of MODIS detected fires in 2011. A similar pattern was observed for each year between 2003-2011. The inset shows fire distribution for all the years (2003-2011) over a small area, 150 km x 150 km in Southern Sudan. Most fires occurred in the savannas and grasslands. b. Spatial distribution of the main types of land cover in the Northern Subsaharan Africa. Barren or sparsely vegetated lands occupy the largest area (25%), followed by woody savannas and grasslands, each at 15% (cf. section 3.1).

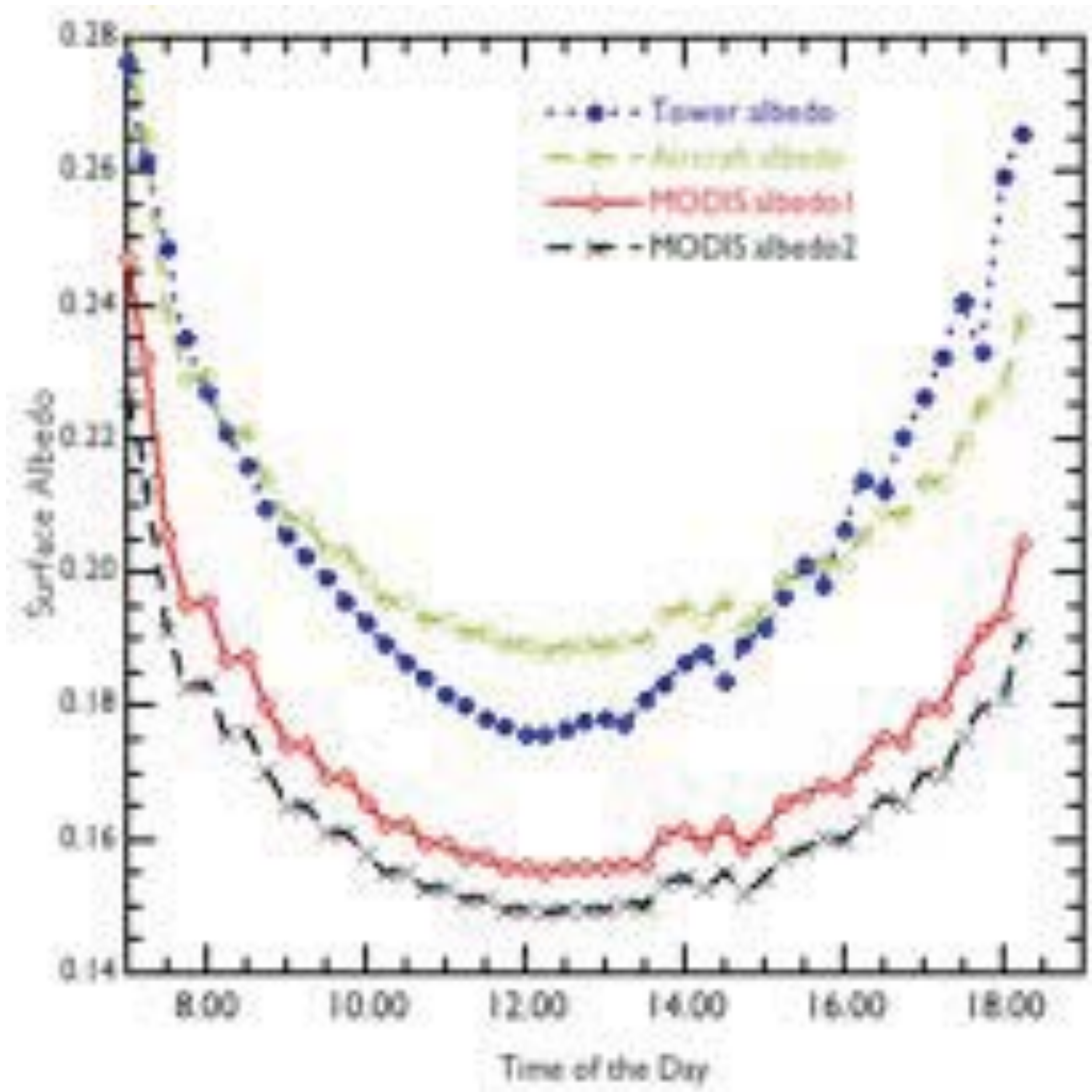

Fig. 2. Comparisons between instantaneous albedos (15-min intervals) derived from airborne CAR, tower-based measurements, and satellite MODIS using two different gap filled approaches over the CART site on 24 June 2007 during CLASIC Field Campaign. The difference between daily average MODIS and Aircraft/Tower albedo varies from 15-20% (cf. Table 1).

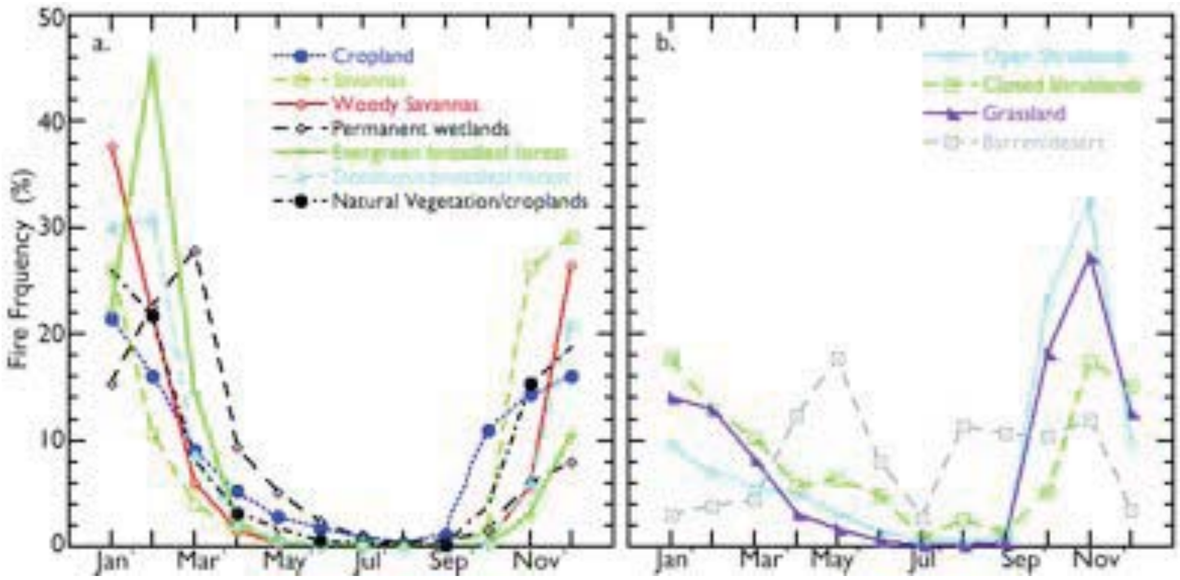

Fig. 3. Monthly Fires detected by MODIS (2003–2011) normalized by the total fires for each land cover type in Northern Sub-Saharan Africa. Most fires occur between October and March with peak for some cover types around a. January, or, b. November. Barren or desert land cover type has a peak around May.

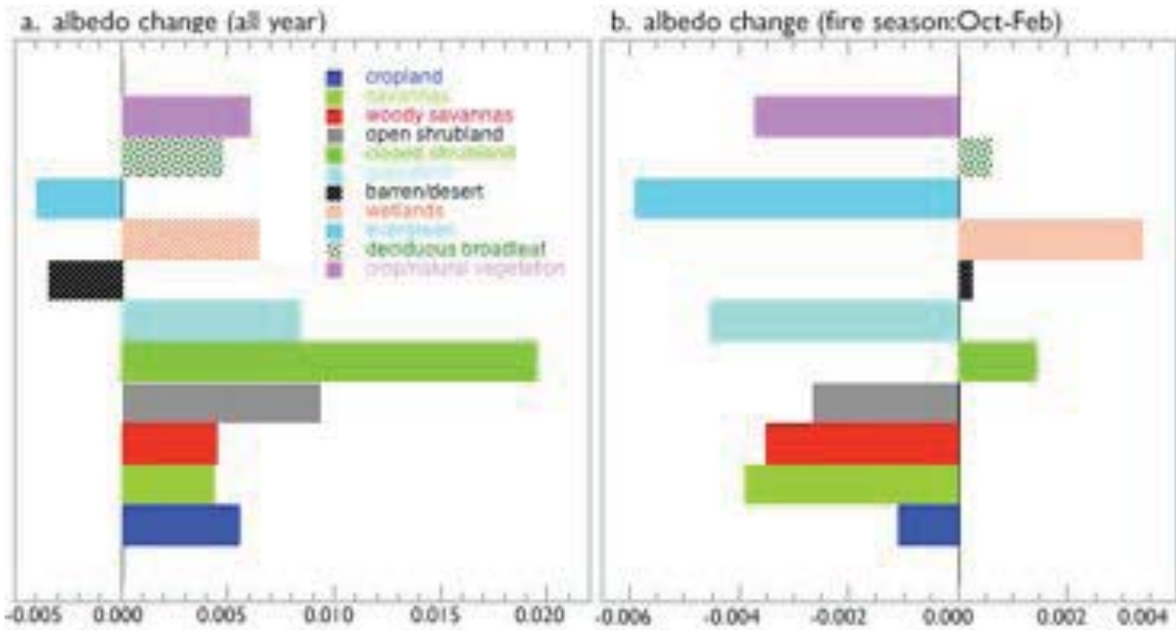

Fig. 4. Annual mean change in albedo for different land cover types averaged over nine years (2003-2011).

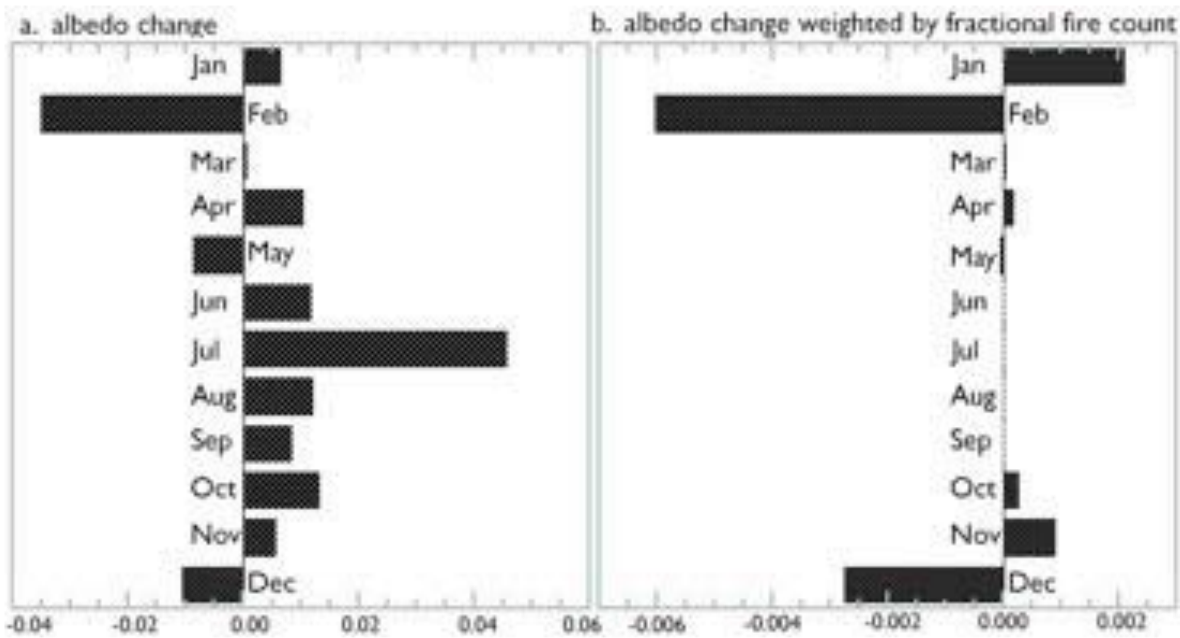

Fig. 5. a. Monthly change in albedo associated with wildfires for all land cover types combined. b. Same as in a., but weighted by fire count observed by MODIS in each month and normalized by total fire count.

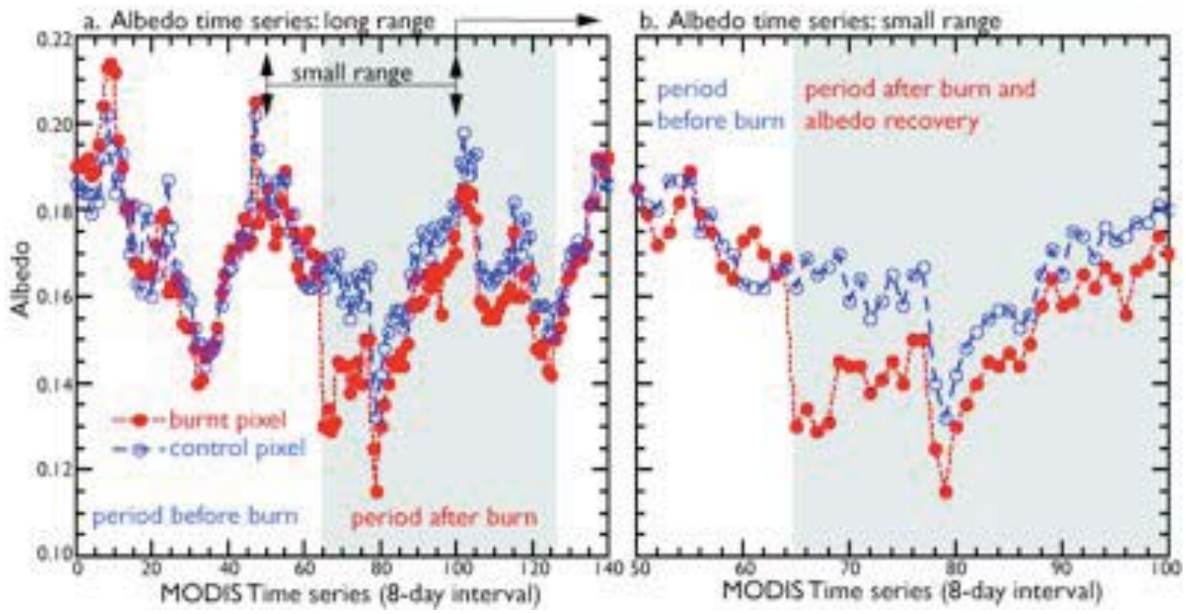

Fig. 6. a. An example of albedo time series of a burned pixel (red line) and its corresponding control pixel (blue line) beginning 10 Feb 2005 to 2 Feb 2008. The gray-shaded area represents mostly the post-fire period. b. Same as a., but zooming into the post-fire period. The control pixel mimics how the burned pixel would have behaved without fire. Fire was detected on 26 June 2006 and its effect on albedo lasted for about 288 days.

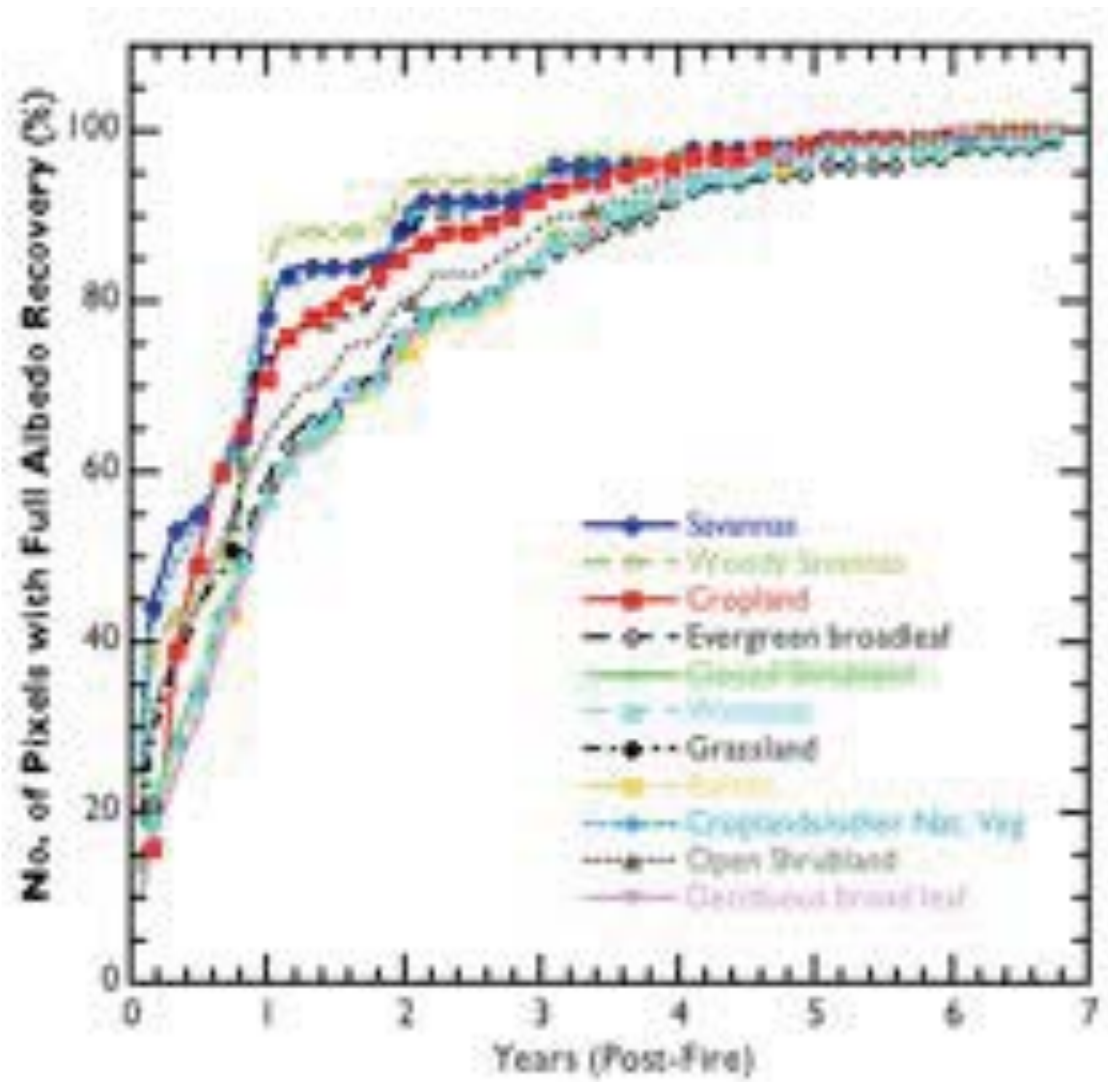

Fig. 7. Percentage of pixels burned in 2003 that has recovered by each subsequent year tracked over a period of seven years for different land cover types in northern sub-Saharan Africa. Points are plotted every 30 days.